A comparative Study on Characteristics of Dynamic Oxide Film of Molten Zn-Al Alloys

M. Divandari* **and M. Mehrabian**

* *divndari@iust.ac.ir*

Received: March 2017 **Accepted: August 2017**

School of Metallurgy and Materials Engineering, Iran University of Science and Technology, Tehran, Iran.
DOI: 10.22068/ijmse.14.3.34

Abstract: *This paper investigates the difference between thickness of zinc-based alloys oxide films in dynamic condition using the oxide-metal-oxide (OMO) sandwich method and static condition by theoretical calculations. In dynamic condition, the thickness of the oxide film in the OMO sandwich sample was characterized by scanning electron microscopy (SEM). In the static condition, the thickness and type of the oxide films were studied based on thermodynamic and kinetic estimations. The results showed that the oxide film thickness in molten Zn4Al and ZA27 alloys using OMO sandwich method was estimated to be in the range of 70-200 nm and 30-100 nm, respectively. However, the thickness of oxide films in the static oxidation based on the theoretical calculations, regardless of melt chemical composition, were about 2-5 nm.*

Keywords: *Zn Alloys, OMO Sandwich Method, Dynamic Oxidation, Static Oxidation, Surface Oxide Film.*

1. INTRODUCTION

When liquid metals and alloys are exposed to air, the surface of the melt oxidises quickly which results in the formation of a solid oxide film in most cases. These can be formed at all stages of the casting process, including melt treatment, handling and pouring. Turbulent flow involved in these processes can entrain the surface film, forming double oxide films, called bifilms[1]. The lack of bonding between the films causes the bifilms to act as cracks in the liquid metal, which result in defective and unreliable castings after solidification. [2–4] Using fluxes or employing inert gases, it is possible to reduce and/or prevent the formation of solid oxide films during melt preparation stage; however, the problem of rapid formation of the detrimental solid oxide films during the pouring has yet to be overcome. The formation and entrainment of the oxide films, especially during this very short stage, can seriously impair the mechanical properties of the casting components [5].

Zinc-Aluminum alloys (ZA series) have a good combination of physical and mechanical properties causing them to be selected in many applications as a substitution to cast irons, aluminum and copper alloys [6]. Mechanical properties of Zn-Al alloys usually increase with increasing Al content, for example the as-cast strength of ZA27 alloy is 440 MPa, which is more than that of the most common industrial cast Al alloys [7]. In addition to ZA series, Zn4Al (ZAMAK3) is one of the most widely used zinc alloys, thanks to its near-to-eutectic composition is of excellent casting properties[8].

In the zinc based alloys, the role of aluminum is mainly to increase strength and reduce the attack by the melt to steel-made components of the casting machine. The latter function is based on the fact that a thin and tenacious oxide readily formed on the melt and through this, no direct contact of the melt and the components take places [1]. However, considering the fact that nearly 80 percent of zinc alloys are cast by high-pressure die casting (HPDC), the high surface turbulence associated with this process is one of the most important phenomena responsible for the entrainment of the surface oxide into the melt [1].

Various researches have shown that the bifilms are able to act as cracks, initiating gas or shrinkage porosity, due to entrapping some air between two oxide layers by folding action upon itself [9–12]. Considering the impact of bifilms on the mechanical properties of the castings,

[DOI: 10.22068/ijmse.14.3.34]

previous researches [13–15] demonstrated that the characteristics of the oxide films are one ofthe basic parameters in detecting behavior of the bifilms, as the thickness and morphology of the oxide films influence the amount of air inside the bifilms. According to Syvertsen, [16] the increase in film thickness leads to the increase in its strength, causing hard folding of the film that promotes the introduction of air into the casting.

The oxide films are, generally, too thin to be observed on polished sections.They havemostly been detectable on the fracture surface [17, 18] which makes investigating their characteristics difficult. It should be noted that the fractographic technique is not capable of detailed inspection of morphology and thickness of the oxide films. However, the OMO sandwich method [19], provides a favorable conditions for investigating thickness and morphology of the oxide films as well as the effect of alloying elements and alsodifferent pouring temperatures on these characteristics.

There are two common approaches forthe estimation of the oxide film thickness using Oxide-Metal-Oxide (OMO) sandwich method, namely folding approach, and side view approach (Fig. 1). Divandari and Campbell [13, 14, 19] investigated thickness of short time oxide films in the Al-5Mg and Al-7Si-Mg alloys using both aforementioned methods. Moreover, Mirak et al. [15] studied oxide film thickness of AZ91 alloy using folding approach. In addition, Azarmehr et al. [20] examined oxide film thickness in the Al-Mg alloys in casting conditions through both

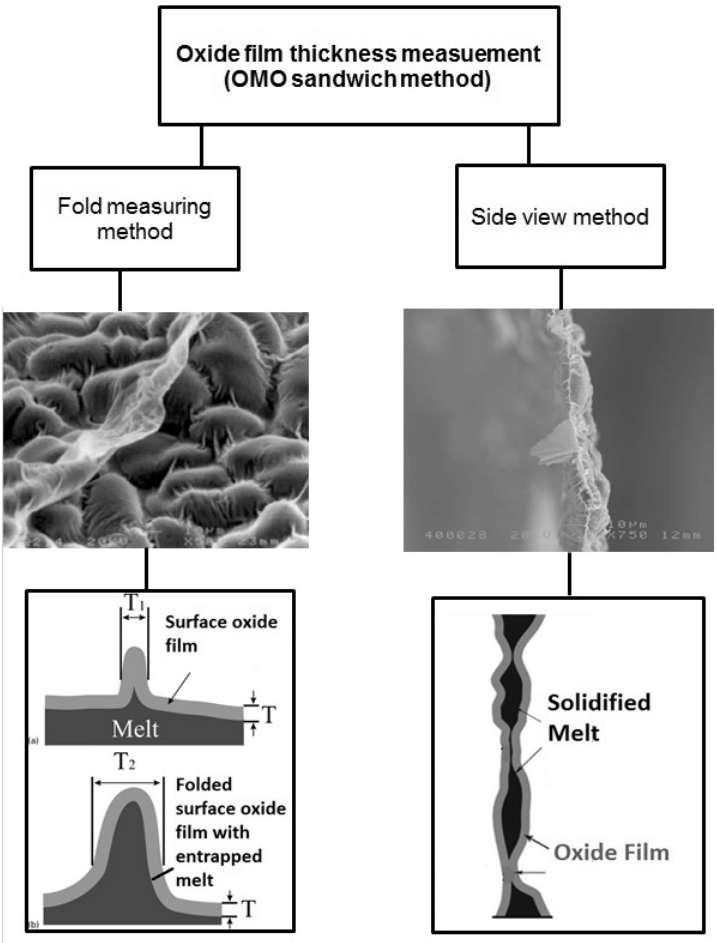

Fig. 1. Schmatic diagram showing two methods used for measuring oxide film thickness in OMO snadwich .

[DOI: 10.22068/ijmse.14.3.34]

approches. The thickness of dynamically formed oxide in pure aluminum was also investigated using folding approach [21].

The main purpose of the current study is to analyze the intentionally created oxide films in Zn4Al and ZA27 by the OMO sandwich method, which is appropriate for simulating the real conditions during the pouring of cast metals into the mold. Furthermore, the formation and growth of the oxide film on the surface of the molten Zn4Al and ZA27 alloys werepredicted by thermodynamic and kinetic calculations. Finally, the two were compared and discussed.

2. EXPERIMENTAL PROCEDURE

Commercial grades of Zn, Al, Cu and Mg ingots were used for preparing ZA27 alloy. Chemical compositions of the alloys are shown in the Table 1. A commercial Zn4Al (ZAMAK3) ingot was used for the experiments.

The Zn4Al and ZA27 alloys were melted in a graphite crucible in a resistance furnace and poured in the temperature range of 703-723 K(430-450 °C) and 823-843 K(550-570 °C), respectively. The melt was poured into a silica sand mold having 8 wt.% sodium silicate as a binder, hardened by CO_2 gas.

To form a steady succession of air bubbles into the melt, air at 1.2 and 2.8 bar (for ZA27 and Zn4Al, respectively) from an air compressor was blown via a silica tube with the inner diameter of 1.5 mm as schematically shown in Fig. 2. The silica tube was inserted approximately 10mm into the casting through the ingate. This location had the advantage of keeping silica tube hot and

Table 1. Chemical compositions of the prepared alloys (Weight Percentage)

Elements	Al	Cu	Mg	Cd	Pb	Mn	Sn	Zn
Zn4Al	4.1	0.038	0.057	0.003	0.006	0.002	0.002	Balance
ZA27	26.32	2.372	0.017	0.002	0.048	0.006	0.028	Balance

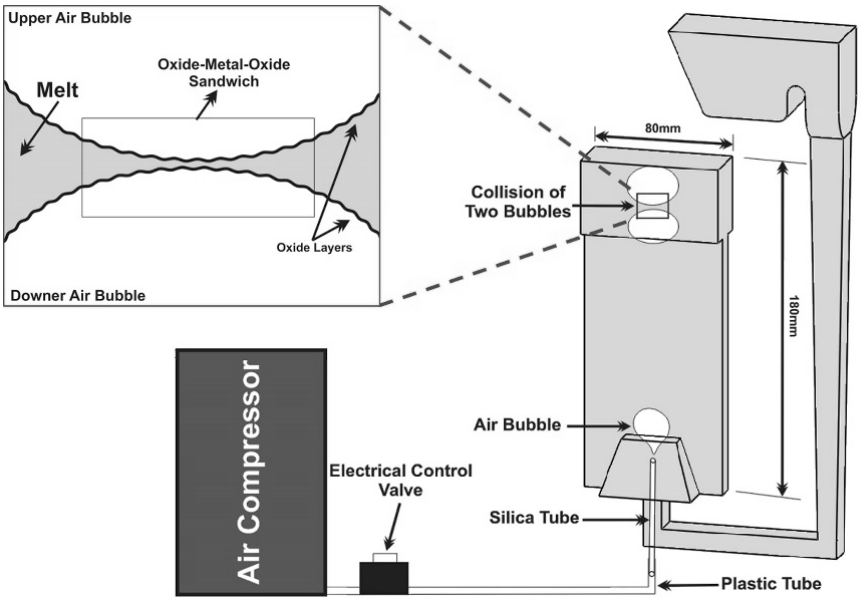

Fig. 2. Experimental setup for creating OMO sandwich samples and a close view of the sandwich.

[DOI: 10.22068/ijmse.14.3.34]

open, preventing obstruction by premature solidification of the melt. Bubbling into the melt could be continued until last moments of pouring and before solidification of casting. This condition was aided by the presence of two trapezoids, enlarging the mold around the tube, retarding solidification and creating better bubbling condition. The solidified castings sectioned to find a suitable OMO sandwich sample to be characterized more thoroughly by TESCAN-WEGA II scanning electron microscopy (SEM) equipped with energy dispersive X-ray spectroscopy (EDS). More details of the experimental procedure can be found elsewhere [19].

3. RESULTS AND DISCUSSION

3. 1. OMO Sandwich Solidification

The specimen used in this research, as shown in Fig. 2, is a triple layer sandwich formed by collision of two bubbles, including two oxide layers and a small amount of entrapped melt between them. A close view of the OMO sandwich is also shown in Fig. 2. Figures 3a and 3b show lateral views of the sandwich in ZA27 alloy. Figs 3c and 3d show the results of EDS analysis from point A and B in the Fig. 3a. The presence of the entrapped melt between two oxide layers is confirmed by EDS analysis from point A. The oxygen peak obtained from point B verified the presence of the oxide layers of the two bubbles. Fig. 3d reveals the interestingly high concentration of aluminum in this region. As can be seen in Fig. 3a, thickness of the OMO sandwich in this alloy, is around 45μm, mainly due to the precense of entrapped metal, which is not helpful for the investigation of the oxide film. However, the sandwich thickness decrease towards the outer edges of the sandwich, permitting individual metal dendrites to be

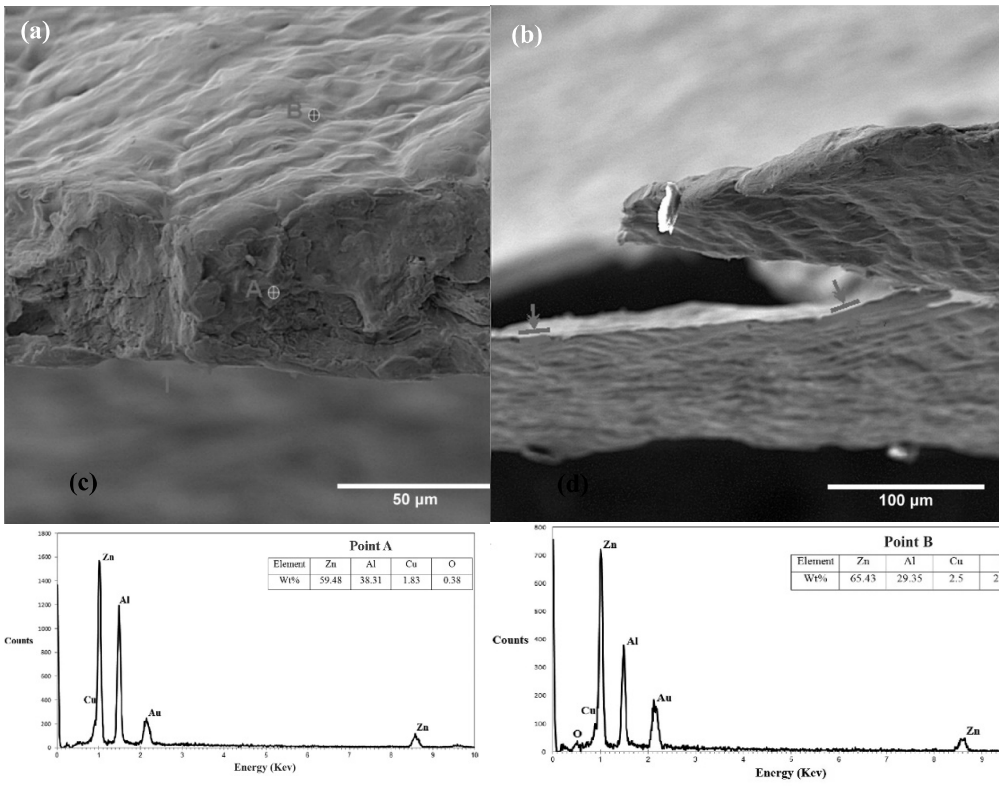

Fig. 3. SEM micrograph of ZA27 alloy representing: (a) sandwich edge; (b) decreasing sandwich thickness towards the outer edges; (c) and (d) EDS analysis taken from point A and B.

[DOI: 10.22068/ijmse.14.3.34]

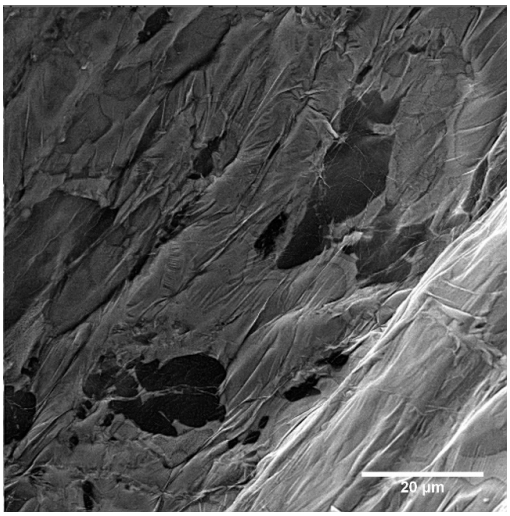

Fig. 4. Close view of SEM image taken from thinner zone of OMO sandwich of ZA27 alloy.

observed as shown in Fig. 3b. This figure shows some regions in OMO sandwich where thickness is reduced to 2.5-3.5µm allowing more details to be seen as shown in Fig. 4.

The part of the side view of the OMO sandwich of Zn4Al alloy is also shown in Fig. 5a. The sandwich thickness, in this case, is in the range of 100-140µm. Fig. 5b shows the result of EDS analysis from the central part of the side view of Zn4Al OMO sandwich and confirms the presence of the entrapped melt between two oxide layers.

During the collision of two bubbles, the liquid metal may be only partially squeezed out between the two impacting bubbles by bouyancy force of the lower bubble. According to Divandari and Campbell [13, 14, 19], during the solidification the volume contraction of melt can

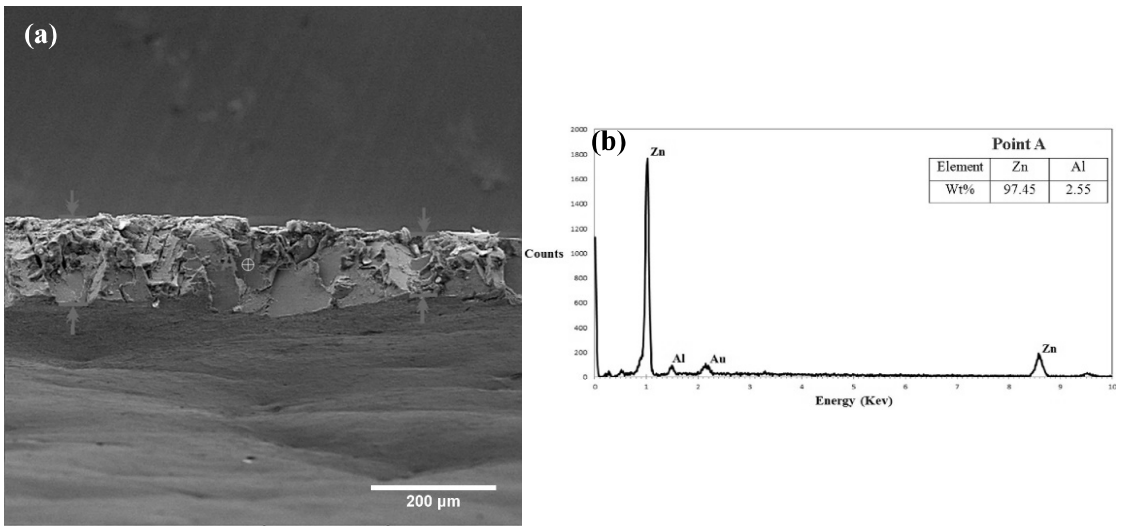

Fig. 5. Side view of OMO sandwich formed in Zn4Al alloy and corresponding EDS analysis from the point A.

[DOI: 10.22068/ijmse.14.3.34]

assist the melt motion between the two bubbles. This phenomenon is particularly observed where, in most case, a nice and clear dentrite structure of solidified metal can be noticed inside OMO sandwich. The solidification regime is discussed schematically in previous researches [20, 21].

It can be noticed that during the solidification, although the thickness of the sandwich is variable due to the dissimilar stresses applied on its different areas, the oxide film thickness increases. These stresses result in variables and wich thickness in the range of 3-45 μm for ZA27 and 100-140 μm for Zn4Al. Figure 5a clearly shows metal grains (confirmed to be metal alloy by analysis in Fig. 5b) with planar fracture surfaces rather like cleavage planes. However, zinc is known to fracture by cleavage, so that there might be an expectation that Zn-4Al alloy would also fracture by cleavage.

The strong effect oflow melting temperature of the alloy and its fast decreasing during the experiment, will, of course, significantly increase the problem of squeezing the liquid metal out from the space between the two bubbles because of increasing the viscosity of the melt.This phenomenon has not been observed in other alloys [13, 14, 19–21]. Consequently, it can be expected that the thickness of the sandwich will vary greatly as shown in the Fig. 3a and Fig. 5a.

3. 2. Determination of stable oxide phase

Liquid Zn4Al alloy is shortly contacted, as arrived into the mold, with an air of 2.8 bar pressure at 703-723 K (430-450 °C). The analysis will be performed at 713 K(440 °C). During the first steps, the oxidation reaction of pure liquid zincat 713 K (440 °C)in an oxygen-containing atmosphere was investigated. Zinc is known to form one stable solid zinc-oxide (ZnO), according to the following reaction:

$$Zn_{(L)} + 0.5\ O_2 = ZnO_{(S)} \quad (1)$$

The Gibbs free energy change of reaction (1) is written as:

$$\Delta_1 G = \Delta_f G^{\circ}{}_{ZnO} - 0.5\ RT\ ln(ln\frac{P_{O_2}}{P^{\circ}}) \quad (2)$$

where $\Delta_f G^{o}_{ZnO}$ (J/mol) is the standard Gibbs free energy of formation of solid zinc oxide from gaseous O_2 and liquid zinc at 713 K (440 °C) (-279.2 kJ/mol [22]), T is the absolute temperature, P_{O2}(bar) is the partial pressure of O_2 in the gas phase, P° is the standard pressure. The solubility of oxygen in liquid zinc is neglected here. Substituting the above values into Eq. (2), the following result is obtained: Δ_1G= -277.6 kJ/mol. The high negative value of Gibbs free energy for this reaction shows strong thermodynamic driving force for the formation of zinc oxide. Thus, pure liquid zinc will be covered by the solid pure ZnO layer under the conditions of the present experiment. Now, by adding some Al to liquid zinc, according to the Al-Zn phase diagram [23], at 713 K (440 °C) the maximum solution of aluminum in liquid zinc is 14 wt.%. Therefore, the Zn4Al at 713 K(440 °C) is a single phase liquid alloy. On the surface of this phase the following redox reaction can take place:

$$3\ ZnO_{(S)} + 2\ Al_{(L)} = Al_2O_{3(S)} + 3Zn_{(L)} \quad (3)$$

The Gibbs free energy change of reaction (3) is written as follows:

$$\Delta_3 G = \Delta_f G^{\circ}{}_{Al_2O_3} + 3\ RT\ ln(\gamma_{Zn} X_{Zn}) - 3\ \Delta_f G^{\circ}{}_{ZnO} - 2\ RT\ ln(\gamma_{Al} X_{Al}) \quad (4)$$

where $\Delta_f G^{\circ}_{Al_2O_3}$ (J/mol) is the standard Gibbs energy of formation of pure Al_2O_3(=-1,452.0 kJ/mol at 713 K(440 °C)[23]), X_{Al} and X_{Zn} are the mole fractions of Al and Zn respectively in the liquid alloy, γ_{Zn} is the activity coefficient of Zn in the liquid alloy (approximately equal to 1 in the diluted solution of Al) and γ_{Al} is the activity coefficient of Al in the liquid alloy. The latter is approximately constant in dilute alloys with γ_{Al}≅3.3 at 713 K(440 °C)[24]. Substituting the above values into Eq. (4), Δ_3 G is negative at 713 K(440 °C), ifXAl> 9.5 · 10-24. This result shows that even the minor Al contamination in liquid zinc will lead to the replacement of the ZnO phase by the Al_2O_3 phase [25]. The 4 wt.% of Al in the Zn4Al alloy is a much larger concentration

[DOI: 10.22068/ijmse.14.3.34]

than this theoretical minimum value, so reaction (3) will take place and the surface of the liquid Zn4Al alloy will be covered by a thin Al_2O_3 layer. Although there is some information in the literature on the formation of complex ZnO. Al_2O_3 oxide(s), [26] their thermodynamic properties are unknown, thus their role is neglected here. However, almost instantly, aluminum atoms will convert firstly formed ZnO ultra-thin layer into an Al_2O_3 layer, based on reaction (3). The time required for this exchange to occur is a matter should be considered. Suppose that the time needed for reaction (3) to completely occur be equal to the diffusion time of aluminum through the liquid zinc layer of 10-1000 nm thickness. The diffusion coefficient of aluminum in the liquid zinc is around D = 10^{-9} m^2/s [27]. Based on the validity of the parabolic Fick law, [28] equation (5) can be applied.

$$L = \sqrt{2 \cdot D \cdot t} \tag{5}$$

Using aforementioned values, t calculated to be 5×10-8-5×10^{-4} s. It is such a short time andit seems safe to assume that the surface of the liquid Zn4Al alloy is covered wholly by an Al_2O_3 layer and does not cover partially by ZnO. It should be noted that in the composition range of Al–5 wt.% Mg, addition of above 1 wt.% Mg causes the precipitation of MgO instead of Al_2O_3 andincreasing time leads to formation of $MgAl_2O_4$ spinel[29]. As the oxidation was dynamic in the present study, and also Mg content was much lower than aforementioned value, the formation of magnesia and spinel is ignored in the calculations.A part of the oxide film is shown in Fig. 6a. The EDS analysis (see Fig-s 6b-c) confirmed that the aluminum concentration along the surface of the alloy is higher than that in the bulk of the alloy [25]. This Al-segregation to the surface is induced by oxidation of the segregated atoms.Obviously the same conclusion follows for the ZA27 liquid alloy with even higher Al-content (see Fig. 3d).

3. 3. Estimation of the Oxide Film Thickness

Following previous discussions, the OMO sandwiches formed in Zn4Al and ZA27 alloys are relatively thick. This makes the side view method in appropriate forexact estimation of the oxide film thickness. Figure 7 shows several parts of the oxide surface in the Zn4Al alloy. In

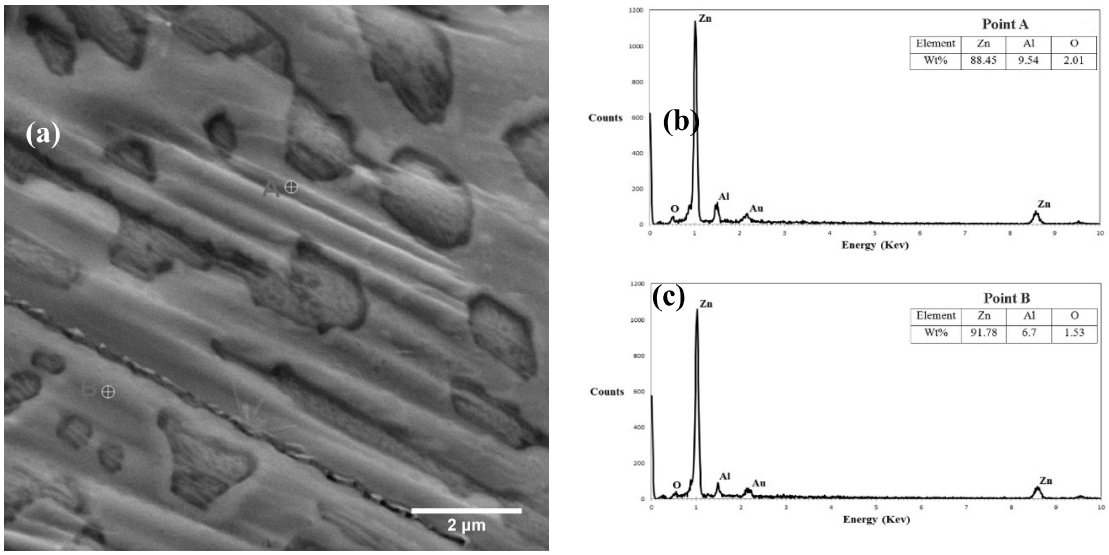

Fig. 6. Surface of the oxide film in Zn4Al alloy and respective EDS analysis from the points A and B.

[DOI: 10.22068/ijmse.14.3.34]

the case of an approximately perpendicular folding to the SEM image, the half of the folding thickness is the approximate thickness of the oxide film [13–15, 20]. As indicated by the markers, the minimum and maximum folding thickness values in Fig. 7a is measured to be 140 nm and 1000 nm respectively, while the corresponding values were 160 nm and 1200 nm in Fig. 7b. These values were also about400 nm and 1300 nm in Fig. 7c and 500 nm and 600 nm in Fig. 7d. Thus, the difference between the minimum and maximum thickness of the folding is large. This is because of the different amounts of entrapped metal between the two oxide layers. It can be explained further by different local stresses in each fold and rigidity of the oxide film [13–15, 20, 21]. It should be added that the apprantly single oxide layers (which are, in fact, double layers oxide film with no metal in between) were found in some locations such as Fig. 7d. These arethe result of complete evacuation of melt between two colliding

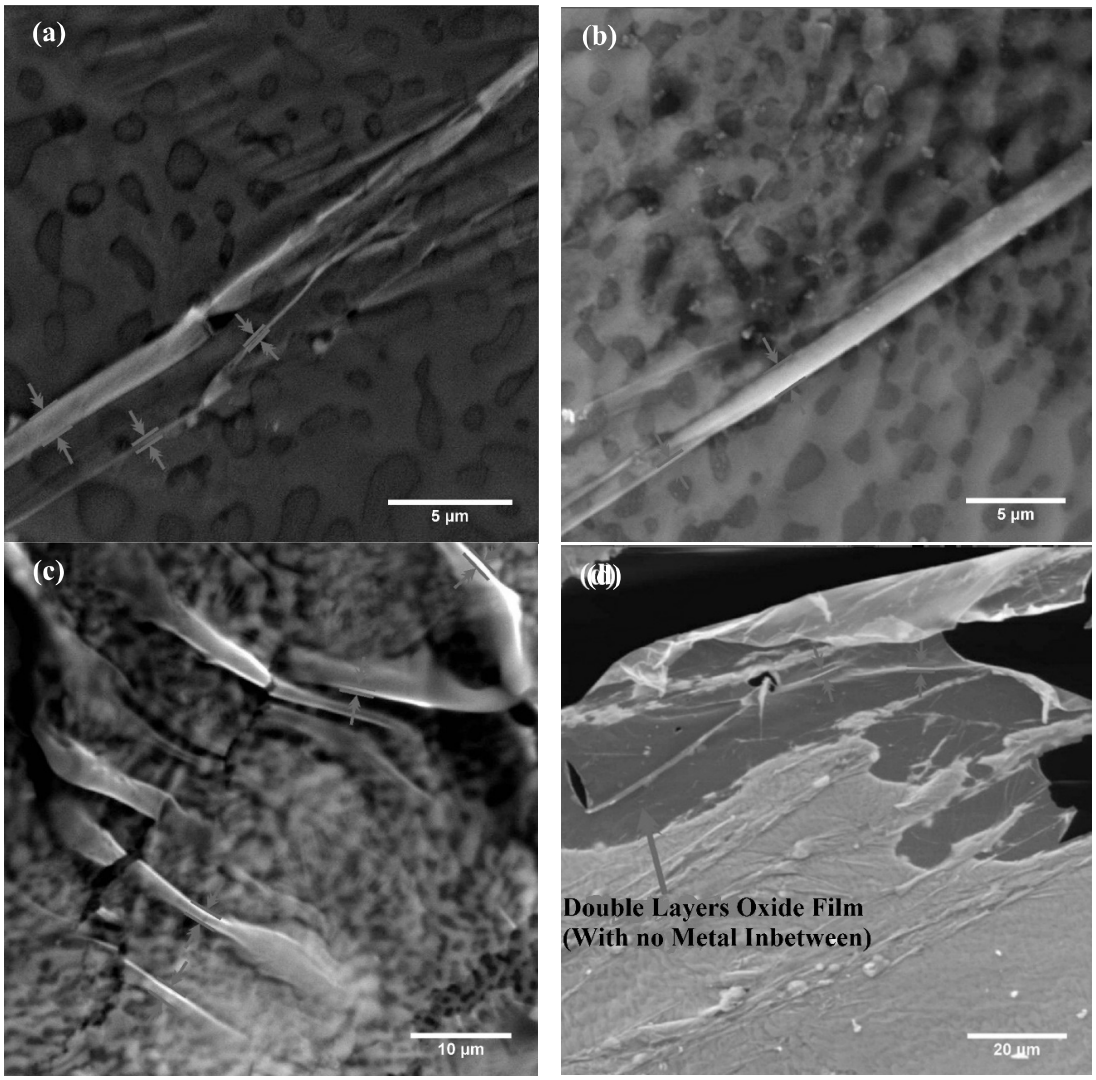

Fig. 7. Suitable folding on the surface of the oxide film in Zn4Al alloy for measuring oxide film thickness in different parts of OMO sandwich.

[DOI: 10.22068/ijmse.14.3.34]

bubbles [14, 19, 20]. To obtain the oxide film thickness one should take into account the minimum folding thickness values. Therefore, it can be stated that the approximate thickness of oxide film in Zn4Al alloy is in the range of 70-200 nm.

The perpendicularly directed folds in the SEM images in ZA27 alloy are shown in Fig. 8. With halving the minimum thickness of these folds, the thickness of oxide film in ZA27 alloy is measured to be in the range of 30-100 nm. These values showthat the thickness of oxide films in both Zn4Al and ZA27 alloys are less than that in previous reports on various film forming alloys, as shown in Table 2 [13, 14, 20, 21]. These differences can generally arise from the difference in the estimating approaches, time and temperature intervals they experincedand impurities. Moreover, it can be attributable to the varying ages of different parts of the oxide film on the rising bubble. It will continuously split and reform, and so might be expected to have a wide variety of ages from a few seconds to several minutes.

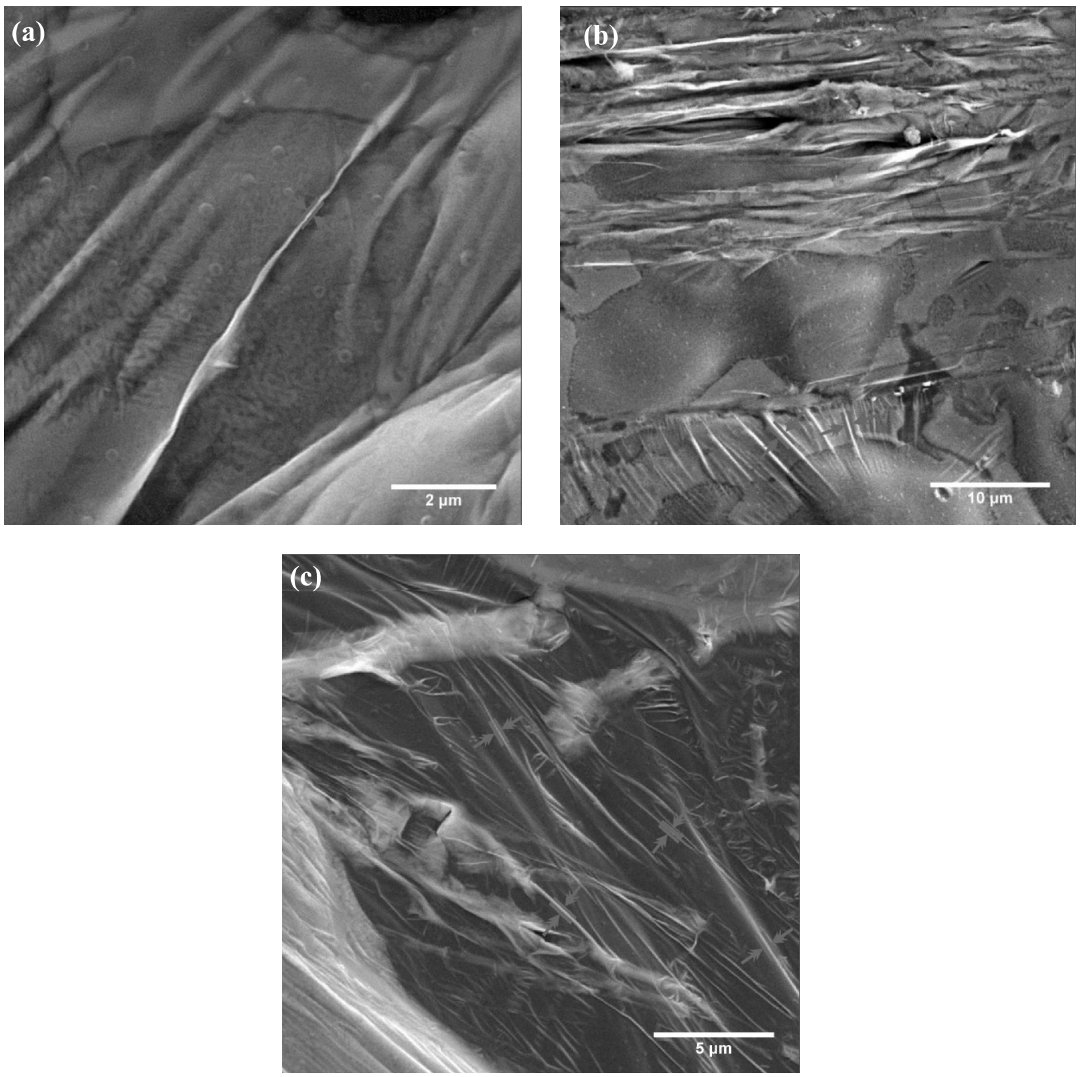

Fig. 8. Suitable folds for measuring the thickness of oxide films in ZA27 alloy.

[DOI: 10.22068/ijmse.14.3.34]

Table 2. Thickness of oxide films formed in different alloys[13,14,20,21].a

Alloy	Oxide film thickness	Reference
Zn4Al	70-200	This work
ZA27	30-100	This work
Pure aluminum	100-500	[21]
Al-7Si-0.4Mg	50- <500	[14]
Al-7Si-0.4Mg	200-500	[21]
Al-1Mg	150-250	[20]
Al-2Mg	200-300	[20]
Al-5Mg	300-800	[13]

As shwon in Table 2, oxide film thickness in Zn4Al and ZA27 alloys are less than Al-Mg alloys. Different thickness values appear to be mainly the result of the chemical composition of oxides. Several researches [30–33] have shown that the presence of non-noble metals like Mg and Ca incorporate in composition of main oxide by forming non-protective and discontinues oxide layers such as MgO and CaO, which significantly increase oxidation and subsequently oxide film thickness. However, aluminum oxide has a good protective characterdue to the desirable Pilling-Bedworth ratio and also low solubility of oxygen. Hence, Feliu and Barranco [34] using XPS analysis showed that the aluminum in zinc improves the oxidation and corrosion behavior of Zn-Al alloys due to segregation toward surface and formation of Al_2O_3 on the outer surface of the alloy. There are also other reports [35–37], based on latter reason,showing substantial improvement of oxidation resistance behavior with addition of aluminum to zinc.

3. 4. Calculation of Thickness Through Kinetic Considerations

It is rather difficult to predict the kinetics of the oxidation process. Determining the thickness of the oxide film in theoretical condition can be obtained through characterizing the kinetics of growth and chemical composition of the oxides. Thickening the oxides at the first stage is controlled by an interface reaction, which is expressed by a linear rate [37]. In the second stage, oxidation takes place at the interface with the involvement of diffusing ions of one of the components and the surface ions of another component, which is described by a parabolic rate [38]. Initially, when the oxide layer is very thin, i.e. in the interface reaction stage, the overall rate of layer formation is only restricted by the rate of chemical reaction. Obviously, this is due to the instantaneous supply of the second component because of the negligibly short diffusion path. However, it could be expected that in the case of protective oxide, this stage is very short, as the diffusion coefficient values of the components in oxide layer are very low. According to Brocket al. [39] the oxidation of solid Al-Zn alloys under similar condition at the temperature range of 748-848 K (475-575 °C) start with the formation of an amorphous Al_2O_3 layer of at least 2.5 nm thickness. Jeurgens et al. [40] have investigated oxidation of pure aluminum at different temperatures and the formation of an amorphous alumina layer at 673 K (400 °C) was reported. The critical thickness for the amorphous Al_2O_3 layer at 673 K (400 °C), before nucleation of crystalline Al_2O_3 layer under amorphous layer, was reported to be about 2-4 nm. A similar result of 5.3 nm is also given else where [41]. Nucleation and growth of crystalline Al_2O_3 layer takes a much longer time (5-10 minutes for nucleation of the γ-Al_2O_3 and about 5 hours for transformation to α-Al_2O_3 when the alloy is in the liquid state [42]), so it could not be expected to take place here due to the short time

[DOI: 10.22068/ijmse.14.3.34]

of oxidation process. In order to estimate the final thickness of oxide layer, at the first it is essential to estimate the time required for a sufficient amount of Al to concentrate in the outer layer of the liquid Zn4Al alloy assuring the formation of a 2.5 nm thick Al_2O_3 layer. Taking into account the density of amorphous Al_2O_3 (3690 kg/m^3[40]), and the density of liquid Zn4Al alloy (6400 kg/m^3 [27]), the diffusion distance of aluminum in the surface layer of the Zn-Al alloy should be at least about 37 nm to assure the formation of a 2.5 nm thick amorphous Al_2O_3. According to the diffusion coefficient of aluminum in the liquid Zn-Al layer (D = 10^{-9} m^2/s [27]), and the parabolic Fick law[28], the time of this process is almost shorter than 10^{-6} s,which sufficesit to say that the outer layer of the Zn4Al alloy is covered by at least a 2.5 nm amorphous alumina layer. Further growth of this amorphous oxide layer will be limited by the diffusion of Al^{3+} ions through this layer [43]. Therefore, the alumina layer is probably an amorphous ultra-thin layer of 2-5 nm in thickness. Now, the thickness of the Al_2O_3 layer at approximately 713 K (440 °C) is estimated as a function of time. It is reasonable to assume that the growth of the oxide layer is limited by the diffusion of Al^{3+} ions through the Al_2O_3 layer. It is also supported by the fact that the diffusion coefficient of Al^{3+} through Al_2O_3 is much higher than that of O^{2-}, [44] due to the smaller size of Al^{3+} ions. On the other hand, the diffusion coefficient of aluminum in liquid zinc is significantly higher than the diffusion coefficient of Al^{3+} in solid Al_2O_3. Then, the thickness of the Al_2O_3 layer as a function of time can be written as [28]:

$$d_{Al_2O_3} \cong \sqrt{2\cdot(0.4)\cdot D_{Al^{3+}}\cdot t} \qquad (6)$$

where $d_{Al_2O_3}$(m) is the thickness of the oxide layer, 0.4 is the mole fraction of Al^{3+} ions in Al_2O_3, $D_{Al^{+3}}$ (m^2/s) is the diffusion coefficient of Al^{3+} ions in the Al_2O_3 layer and t (s) is the exposure time of the Zn-Al liquid to the oxygen-containing gas. If Eq. (6) provides a thickness value smaller than 2 nm, then the actual thickness of the layer is estimated to be within 2 nm to 5 nm. Although at a low temperature of 713 K (440 °C) and 833 K (560 °C) for Zn4Al and ZA27 respectively, no experimental data are available for the diffusion coefficient of Al-ions in alumina; however, its value can be estimated from high-temperature measurements [45]as:

$$\ln D_{Al^{3+}} \cong 10.7 - (72000/T) \qquad (7)$$

Substituting T = 713 K (440 °C) and 833 K (560 °C) into Eq. (7): $D_{Al^{+3}} \cong 6.18\cdot10^{-40}$ m^2/s and $1.28\cdot10^{-33}$ m^2/s for Zn4Al and ZA27 alloys, respectively. Substituting this value into Eq. (6), the critical times, needed to produce $d_{Al_2O_3}$=$2\cdot10^{-9}$ m are 8 ·1021 s and 2.3 ·1015 s. These unreasonable values show that Eq. (7) should not be used for extrapolations to low temperatures. However, it is also deduced that the diffusional growth of the layer is negligible. Subsequently, it seems that the calculated total thickness of Al_2O_3 layer in both alloys is in the range of 2-5 nm.

3. 5. Comparing the Estimation Methods

The difference between obtained values with OMO sandwich and kinetic assessments shows that the experimental condition is significantly different from the assumed condition for the theoretical calculations. This is mostly due to the ignoring the effect of turbulence in theoretical calculations, i.e. due to the so-called "dynamic oxidation condition" during the mold filling process. In casting condition many parameters such as pouring temperature, pouring time, the chemical composition of the alloy, mold periphery and melt flow are capable of influencing the rate and behavior of oxidation. As soon as the bubble enters to the bulk of molten metal, a thin oxide layer forms on air/melt interface. Since thereis perfect atomic contact between oxide and molten metal, any stresses applied to the melt directly reacts onthe oxide layer. Mainly the so-called Reynolds' stresses (initiating from theturbulent nature of the melt flow) in casting processes can extremely affect the structure of this thin oxide layer and leads to

[DOI: 10.22068/ijmse.14.3.34]

many ruptures on it. These ruptures result in exposing fresh surface of molten metal to air. These phenomena providing higher surface area and reaction sites subsequently increase the reaction rate. Aforementioned condition is more dramatic in the case of non-protective oxide layers such as MgO and CaO [20, 31–33, 46]. These ruptures also happen because of applying thermal stresses from the first moment of starting solidification due to the difference between thermal expansion coefficients of melt and oxide. Wightman and Fray [47] stated that the stagnant melt oxidation (static oxidation) is 60 times slower than the dynamic oxidation, which is in agreement with our findings: 2–5 nm (stagnant theoretical condition) versus 30-100 nm and70-200 nm (turbulent experimental condition). Similarly, Berman and Epstein [35] confirmed the same difference considering the reaction rate constant in the static and dynamic oxidation with studying pure liquid zinc through bubbling of water vapor.

4. CONCLUSIONS

1. The turbulent nature of the melt flow, in many casting processes, assist the formation of considerable quantities of folded and double oxide films, bifilms, which adversely affect the reliability of castings. In the current research, oxide filmsintentionally created in Zn4Al and ZA27 by the OMO sandwich method, which is appropriate for studyingthe realturbulent condition effects onthe characteristics of oxide films, were studied.
2. Thermodynamic examinations showed that the most stable oxide phase on the surface of the Zn4Al and ZA27 alloys is the aluminum oxide. Experimental results showed that the side view method in the case of zinc-based alloys is not capable of accurate estimation of oxide layer thickness. Subsequently, the thickness of the oxide films in Zn4Al and ZA27 alloys based on halving the thickness of a fold is estimated to be within the range of 70-200 nm and 30-100 nm, respectively.
3. The thickness of the oxide films forming in Zn4Al and ZA27 alloys through kinetic considerations were identical and estimated to be in the range of 2-5 nm, showing the intense effect of turbulent melt flow on the oxidation behavior of cast alloys.

ACKNOWLEDGEMENT

I would like to express my deep and sincere gratitude to Prof. Jeorge Kaptay for his contribution on theoretical considerations on the oxide film kinetics and also to Prof. John Campbell and Prof. S. M. A. Boutorabi for interesting discussions. Financal support and the grant (160-1240-Y-940115) of deputy of researchof the Iran University of Science and Technology (IUST) is also acknowledged.

REFERENCES

1. Campbell, J., “Complete casting handbook, metal casting processes, metallurgy”, techniques and design. Butterworth-Heinemann, 2015, 24-28.
2. Eisaabadi Bozchaloei, G., Varahram, N., Davami, P. and Kim, S. K.,"Effect of oxide bifilms on the mechanical properties of cast Al–7Si–0.3 Mg alloy and the roll of runner height after filter on their formation". Materials Science and Engineering: A 2012, 548, 99–105.
3. Campbell, J. "An overview of the effects of bifilms on the structure and properties of cast alloys", Met. and Mat.Trans. B, 2006, 37, 857–63.
4. Tiryakioğlu, M., Campbell, J., Nyahumwa, C., "Fracture Surface Facets and Fatigue Life Potential of Castings", Met. and Mat.Trans. B 2011, 42, 1098–103.
5. Campbell, J.,"Sixty Years of Casting Research", Met. and Mat. Trans. A, 2015, 46, 4848–53.
6. Kaplan, M., İleriturk, M., Balalan, Z., "Relationship Between Microstructure, Hardness, XRD, TGDTA Analysis, and Wear Performance of a Cast ZA Alloy", Mat. and Manufac. Processes, 2008, 23, 400–6.
7. Gervais, E., Barnhurst, R. J., Loong, C. A.,"An Analysis of Selected Properties of ZA Alloys", JOM, 1985, 37, 43–7.
8. ASM Handbook, Vol. 2, ASM International,

[DOI: 10.22068/ijmse.14.3.34]

Metals Park, OH, 1990, 1623-27.
9. Cao, X. and Campbell, J., "The solidification characteristics of Fe-rich intermetallics in Al-11.5Si-0.4Mg cast alloys",Met. and Mat. Trans. A,2004, 35, 1425–35.
10. Griffiths, W. D., Raiszadeh, R., "Hydrogen, porosity and oxide film defects in liquid Al", J. of Materials Sci. 2009, 44, 3402–7.
11. Raiszadeh, R., Griffiths, W. D.,"The Effect of Holding Liquid Aluminum Alloys on Oxide Film Content",Met. and Mat. Trans. B, 2011, 42, 133–43.
12. Griffiths, W. D., Lai, N. W. "Double Oxide Film Defects in Cast Magnesium Alloy",Met. and Mat. Trans. A, 2007, 38, 190–6.
13. Divandari, M., Campbell, J., "Morphology of oxide films of Al–5Mg alloy in dynamic conditions in casting", Int.Journal of Cast Met. Res.2005, 18, 187–92.
14. Divandari, M., Campbell, J. "Oxide film characteristics of Al-7Si-Mg alloy in dynamic conditions in casting",Int. Journal of Cast Met. Res., 2004, 182-187.
15. Mirak, A. R., Divandari, M., Boutorabi, S. M. A., Campbell, J. "Oxide film characteristics of AZ91 magnesium alloy in casting conditions", Int. Journal of Cast Met. Res., 2007, 20, 215-220.
16. Syvertsen, M. "Oxide skin strength on molten aluminum", Met. and Mat.Trans. B, 2006, 37, 495–504.
17. Campbell, J. "Entrainment defects", Mat. Sci. and Tech. 2006, 22, 127–45.
18. Knott, J. "Commentaries on "Entrainment defects"" by J. Campbell. Mat. Sci. and Tech. 2006, 22, 999–1008.
19. Divandari, M. Campbell, J. "A new technique for study of aluminum oxide films. Aluminum Transactions, 2000, 233–8.
20. Azarmehr, S. A., Divandari, M., Arabi, H. "Investigation on thickness of short time oxide films in Al-1Mg and Al-2Mg alloys", Mat. Sci. and Tech. (United Kingdom) 2012, 28, 1295-1300.
21. Nayebi, B., Divandari, M. "Characteristics of dynamically formed oxide films on molten aluminium", Inter. J. of Cast Metals Res., 2012, 25, 270-276.
22. Barin, I. "Thermochemical Data of Pure Substances", Parts I and II. Verlagsgesellschaft, Weinheim, 1989.
23. Massalski, T. B., Okamoto, H., Subramanian, P. R., Lacprzak. K,. "Binary Alloy Phase Diagrams", 2nd ed. ASM International, 1990.
24. Predel, B., "Phase Equilibria, Crystallographic and Thermodynamic Data of Binary Alloys," vol. 5,. Landolt-Börstein,, 1991.
25. Levai, G., Godzsák. M, Török, T. I., Hakl, J., Takáts, V., Csik, A., "Designing the Color of Hot-Dip Galvanized Steel Sheet Through Destructive Light Interference Using a Zn-Ti Liquid Metallic Bath", Met. and Mat.Trans. A 2016, 47, 3580–96.
26. Toropov, N., Barzakovskii, V.,Lapin, V., and Kurtseva N. "Phase Diagrams of Silicate Systems". Nauka, Leningrad, 1969.
27. Iida, T., Guthrie R. I. "The Physical Properties of Liquid Metals". Oxford University Press, 1988.
28. Poirier, D. R., Geiger, G. H., "Transport Phenomena in Materials Processing". Wiley, 1998.
29. Scamans, G. M., Butler, E. P. "In situ observations of crystalline oxide formation during aluminum and aluminum alloy oxidation", Met. Transactions A 1975, 6:2055–63.
30. Kumari, S. S. S., Pillai, R. M., Pai, B. C. "Role of calcium in aluminium based alloys and composites", Inter. Mat. Reviews 2005, 50, 216–38.
31. Ozdemir, O., Gruzleski, J. E., Drew, R. A. L. "Effect of low-levels of strontium on the oxidation behavior of selected molten aluminum-magnesium alloys". Oxidation of Metals 2009, 72, 241–57.
32. Haginoya, I., Fukusako, T. "Oxidation of molten Al-Mg alloys", Trans. of the Japan Institute of Metals 1983, 24, 613–9.
33. Cochran, C.N., Belitskus, D. L., Kinosz, D. L. "Oxidation of aluminum-magnesium melts in air, oxygen, flue gas, and carbon dioxide", Met.Trans. B 1977, 8, 323–32.
34. Feliu, S. and Barranco, V., "XPS study of the surface chemistry of conventional hot-dip galvanised pure Zn, galvanneal and Zn–Al alloy coatings on steel", Acta Materialia 2003, 51, 5413–24.

[DOI: 10.22068/ijmse.14.3.34]

35. Berman, A., "The kinetics of hydrogen production in the oxidation of liquid zinc with water vapor", Inter. J. of Hydrogen Energy 2000, 25, 957–67.
36. Vasil'eva, S. S., Azhogin, F. F., Shchuchkin, A. I. "Influence of aluminum additions to molten zinc on the corrosion resistance of iron-based alloys", Soviet Mat.Sci., 1984, 19, 493–5.
37. Branson, D. L. "Kinetics and Mechanism of the Reaction Between Zinc Oxide and Aluminum Oxide". J. of the American Cer. Soc., 1965, 48, 591–5.
38. Wallwork, G. R., "The oxidation of alloys", Reports on Progress in Physics 1976, 39, 401.
39. Brock , A. J., Irani, G. R., Pryor, M. J. "The kinetics of the oxidation of aluminum-zinc alloys in oxygen at high temperature", Oxidation of Metals 1981, 15, 77–100.
40. Jeurgens, L. P., Sloof, W., Tichelaar, F., Borsboom, C. and Mittemeijer, E. "Determination of thickness and composition of aluminium-oxide overlayers on aluminium substrates". App. Surface Sci. 1999, 144–145, 11–5.
41. Jeurgens, L., Sloof, W., Tichelaar, F., Mittemeijer, E. "Thermodynamic stability of amorphous oxide films on metals: Application to aluminum oxide films on aluminum substrates", Physical Review B 2000, 62, 4707–19.
42. Raiszadeh, R., Griffiths, W. D. "A method to study the history of a double oxide film defect in liquid aluminum alloys", Met.and Mat. Trans. B 2006, 37, 865–71.
43. Jeurgens, L. P. H., Sloof, W. G., Tichelaar, F. D. and Mittemeijer, E. J. "Growth kinetics and mechanisms of aluminum-oxide films formed by thermal oxidation of aluminum", J. of Applied Phy. 2002, 92, 1649–56.
44. Van Orman, J.A., Crispin, K.L. "Diffusion in Oxides. Reviews in Mineralogy and Geochemistry", 2010, 72, 757–825.
45. Zahidkova, T. Physicochemical Properties of Oxides. Moscow: Metallurgiya, 1978.
46. Lee, D. B., Hong, L. S., Kim, Y. J. "Effect of Ca and CaO on the High Temperature Oxidation of AZ91D Mg Alloys,. Mat. Trans. 2008, 49, 1084–8.
47. Wightman, G., Fray, D. J. "The dynamic oxidation of aluminum and its alloys". Met. Trans. B, 1983, 14, 625–31.

[DOI: 10.22068/ijmse.14.3.34]